PHYSICAL REVIEW B VOLUME 32, NUMBER 10 15 NOVEMBER 1985

Electrical properties of dislocations and point defects in plastically deformed silicon

P. Omling and E. R. Weber*
Center for Advanced Materials, Lawrence Berkeley Laboratory, University of California, Berkeley, California 94720

L. Montelius
Department of Solid State Physics, University of Lund, Box 118, S-221 00 Lund, Sweden

H. Alexander and J. Michel
Abteilung für Metallphysik, II Physikalisches Institut, University of Cologne, D-5000 Cologne, West Germany
(Received 9 May 1985)

Energy levels of defect states introduced by plastic deformation of n-type silicon have been studied by capacitance transient spectroscopy. From the observed properties of the defects, it is concluded that two different types of defects are produced. The first type is interpreted as point defects located in the vicinity of, or inside, dislocations. These deep-level defects have been analyzed in a model involving level broadening due to strain fields and/or defect interaction. The analysis gives information on thermal emission rates, capture cross sections, ionization energies, and deep-level broadenings. In addition, this analysis allows for the determination of accurate defect concentrations. From the improved concentration measurements it has been possible to determine the dependence of the repulsive potential (responsible for the unusual capture mechanism) on the filling times during the capture process. The second type of defects seems to be directly related to dislocations, but their physical properties could not be determined unambiguously. Comparison of the deep-level transient spectroscopy (DLTS) and EPR results allowed tentative identification of the different DLTS lines with particular EPR spectra, and thus conclusions about the microscopic models for different defects. The quantitative comparison of defect concentrations measured by DLTS and EPR also suggests that in strongly deformed silicon, part of the EPR lines might be broadened due to imperfections in the lattice surrounding the paramagnetic center.

I. INTRODUCTION

Plastic deformation of silicon produces a complex spectrum of lattice defects, many of which are connected with energy levels deep in the band gap.[1–9] The dislocations generated can be straight, heavily kinked or jogged, clean, or decorated with impurities, and are generally dissociated into partials with stacking faults in between, to name a few possibilities. In addition to dislocations, point defects and point-defect clusters, generated during the dislocation motion or by dislocation interaction, can be formed. All of these imperfections can be electrically active, and it is well established that plastic deformation results in the appearance of donor as well as acceptor states. The electrical behavior of these defects has, in the past, been studied by rather unspecific methods like Hall effect and photoconductivity, which resulted in a picture of delocalized states in the core of the dislocations.[10] However, the recent use of spatially resolved[8] and of spectroscopic techniques allows us to determine the microscopic nature of these electrically active defects. Electron-paramagnetic-resonance (EPR),[11–14] deep-level transient spectroscopy (DLTS),[2–7] and photo-luminescence[15–17] measurements have been used to obtain a more detailed picture, where both unpaired electrons ("dangling bonds") and deep-level defects have been found in the dislocations as well as in the point defects formed during the deformation. Thus, the fundamental question seems to be at present the microscopic identification of the defects involved, and the correlation of these defects with the properties observed with various techniques.

The EPR technique has proven to be the most successful technique for the identification of lattice defects in semiconductors, especially silicon. EPR of dislocated silicon has been reported in papers from various groups,[11–14] of which two[11,13] agree in their analysis of the EPR signals as being due partly to dangling bonds in dislocations and partly to point-defect clusters. DLTS measurements, which give information only on the deep levels located in the band gap, showed in plastically deformed (PD) silicon a complex spectrum of broadened lines, which all show very unusual nonexponential capture behavior.[4–7] Recently, a first attempt[6] has been made to correlate the various EPR and DLTS spectra, based mainly on a comparison of formation and annealing behavior of the different defects.

The purpose of this paper is to present a detailed study of the deep energy levels produced in plastically deformed n-type silicon. DLTS data will be presented, showing how the electrical properties change with different deformation and annealing procedures. It will also be shown how a complete analysis of some of the DLTS lines gives detailed information on the physical properties of the defects and allows to suggest the type of defect (point defects or dislocations) studied. The properties of these deep levels will be compared with data on EPR centers, and from a comparison of formation behavior, annealing behavior, photo-EPR results, and concentration measurements, we will, finally, suggest microscopic models for some of the centers.

 ©1985 The American Physical Society

II. EXPERIMENTAL

For the experiments, n-type float-zone silicon single crystals (Wacker-Chemitronic) were used, with doping levels of $(1-10)\times10^{15}$ (phosphorus atoms)/cm^3. The grown-in dislocation density was $(1-5)\times10^4$ cm^{-2}. Plastic deformations were made by static compression along [213] in a reducing atmosphere of forming gas (92 vol % N_2, 8 vol % H_2). "Standard" deformations were performed at 650 °C with a resolved shear stress of 30 MPa. High-stress deformations yielding a high concentration of straight dislocations[18] were performed with 300 MPa at 420 °C, after a predeformation at 850 °C. Experimental details of the sample preparation and deformation procedure have been described previously.[19]

Schottky diodes were produced by evaporating Au Schottky contacts and Ga-Al alloy Ohmic contacts on freshly etched crystals. The diodes were characterized by I-V and $1/C^2$-V measurements and only diodes with low leakage current, homogeneous doping profiles, and low series resistance were used for further investigation.

The deep-level emission studies were performed with the DLTS system described in Ref. 20. For capture-cross-section measurements two different DLTS systems were used. For filling pulses larger than 100 ns the system in Ref. 20 was used, but for smaller filling pulses a specially designed DLTS system, which is almost 50-Ω matched, was used. This system consists of a fast pulse generator which has rise and fall times of less than 250 ps with a maximum amplitude of 50 V. This slightly modified pulse generator provides a variable pulse frequency from 1 to 500 Hz as well as single-shot ability. The capacitance transient, which is measured with a Boonton 72B capacitance meter, is sampled at the end of the transient, and this value is subtracted from the next transient, providing a capacitance signal with a dc level around zero. This signal is sampled with a double boxcar analyzer. In the sample holder, as close as possible to the diode, are two microrelays which, during the pulse, disconnect the LO terminal of the C meter to avoid overload and connect the HI terminal to ground, thus giving the sample a good ground connection. Also included is a current probe with a rise time of less than 250 ps that measures the current through the diode. The voltage and current over a typical diode used in this investigation is shown in Fig. 1. From such figures it is possible to determine directly the shortest pulses that can be used for capture measurements with respect to the diode RC constant.

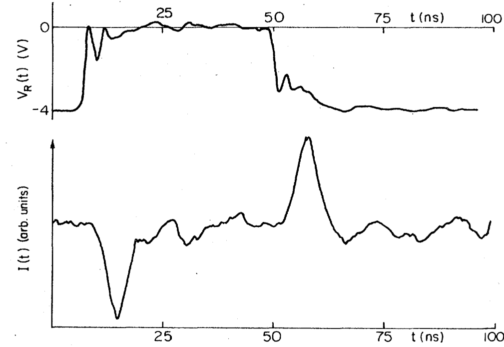

FIG. 1. The measured voltage across the diode and the measured current through the diode for a 42.5-ns filling pulse. The half-width value of the current spike is related to the RC product of the sample, which for this sample gives an RC product of 2.2 ns. The shortest useful pulse width for this sample is therefore ≈ 10 ns.

III. ELECTRICAL MEASUREMENTS

A. Theoretical background

For a level deep in the band gap the energy position, thermal emission rate $e_{n,p}$, and capture cross section $\sigma_{n,p}$ are related by the expression derived from the principle of detailed balance:[21]

$$e_{n,p}=\sigma_{n,p}\langle v_{\text{th}}\rangle N_{c,v}\exp(-\Delta G_{n,p}/kT)\ . \tag{1}$$

Here, $N_{c,v}$ is the effective density of states in the conduction band or valence band, $\langle v_{\text{th}}\rangle$ is the average thermal velocity of the charged carrier, and $\Delta G_{n,p}$ is the change in the Gibbs free energy needed to emit an electron or hole from a deep defect center. The relation between the change in Gibbs free energy, the change in enthalpy ΔH, and the change in entropy ΔS, at constant temperature is given by the thermodynamic relationship

$$\Delta G_{n,p}=\Delta H_{n,p}-T\Delta S_{n,p}\ . \tag{2}$$

If corrections for the temperature dependence of the capture cross section $\sigma_{n,p}$ are made, and it is observed that $\langle v_{\text{th}}\rangle N_{c,v}$ is proportional to T^2, it follows from Eqs. (1) and (2) that the enthalpy is obtained from an Arrhenius plot, i.e., $\log(e_{n,p}/\sigma_{n,p}T^2)$ versus $1/T$. If the capture cross section is temperature independent, the prefactor A_{pf} $[=\sigma_n\langle v_{\text{th}}\rangle N_c\exp(\Delta S/k)]$ can be used to calculate the entropy term, and ΔG can be obtained from Eq. (2).

A convenient method of obtaining data on the thermal emission rates and capture rates is the space-charge techniques.[22] Using these techniques the change in the capacitance signal caused by a change in the electron occupancy of a deep energy level in the space-charge region of a junction barrier can be used to measure absolute values of $e_{n,p}$ and $\sigma_{n,p}$. The capacitance of a n-type Schottky junction is

$$C(t)=\tfrac{1}{2}[A^2q\epsilon\epsilon_0N_i/2(V_D+V_R)]^{1/2}\ , \tag{3}$$

where A is the area, $\epsilon\epsilon_0$ the dielectric constant, V_D the diffusion voltage, V_R the reverse bias, and $N_i=N_D+N_T-n_T(t)$ the concentration of ionized defects. N_D is the shallow doping concentration, N_T the deep-level concentration, and $n_T(t)$ the concentration of deep levels occupied by electrons. The time-dependent change of the capacitance after a zero bias pulse (i.e., all traps filled with electrons in an n-type Schottky diode) is $(N_T \ll N_D)$

$$C'(t)=\tfrac{1}{2}[A^2q\epsilon\epsilon_0/2(V_D+V_R)N_D]^{1/2}\times N_T[1-\exp(-e_nt)]\ . \tag{4}$$

When using DLTS,[23] this capacitance transient is sampled by two gates (boxcar DLTS) at times t_1 and t_2, and the

difference $\Delta C = C(t_1) - C(t_2)$ is monitored as a function of temperature. This gives one peak for each deep level, where the peak position T_{max} corresponds to

$$e_n = \ln(t_2/t_1)/(t_2 - t_1) .$$

By changing t_1 and t_2 the peak position (T_{max}) will shift and e_n can be obtained as a function of temperature.

The concentration of deep levels is obtained from Eq. (4), but using DLTS the convention is to calculate N_T from the equivalent expression

$$N_T = (2/\alpha) N_D (\Delta C_{max}/C_0) , \quad (5)$$

where C_0 is the total capacitance from the junction, ΔC_{max} the maximal DLTS signal, and α a correction factor introduced by the procedure for the sampling of the exponential transient. For a more accurate determination of the concentrations, the influence of the free-carrier tail (sometimes referred to as the λ volume) extending from the neutral region into the space-charge region has to be included. In this case N_T is modified by dividing Eq. (5) by[24]

$$\beta = 1 - [2\lambda / W(V_R)][1 - C(V_R)/C(V_0)] - [C(V_R)/C(V_0)]^2 . \quad (6)$$

Here, β is the part of the space-charge region (W) where the Fermi level is above the deep energy levels and V_0 is the voltage during the filling pulses.

In many cases it has been noted that the observed transients are, for nontrivial reasons, nonexponential, which gives a broadening in the measured DLTS peak.[25] This is particularly true for defects in plastically deformed semiconductors.[5] Thermal emission rates and activation energies deduced from DLTS measurements in these systems are therefore often questioned. However, it has recently been shown that using a model of broadened deep levels (e.g., due to varying alloy composition in the crystal), Eq. (4) will be replaced by[25]

$$C'(t) = \int_0^\infty g(E_{ai}) C_0 \exp[-e_n(E_{ai})t] dE_{ai} , \quad (7)$$

where the (Gaussian) distribution function around the mean energy value E_{a0} is

$$g(E_{ai}) = [1/S(2\pi)^{1/2}] \exp[-(E_{ai} - E_{a0})^2/2S^2] . \quad (8)$$

Here, $2S(2\ln 2)^{1/2}$ is the full-peak half-width (FPHW) of the broadening of the energy level. In this model the thermal emission rates and activation energies can be deduced as in conventional DLTS spectroscopy (one observes the mean energy E_{a0} in the distribution), even though the transients are strongly nonexponential. Furthermore, the energy distribution and the corrected deep-level concentration can be calculated from the observed DLTS spectrum. Even though the application and verification of the model has been performed in alloys,[25] it has been predicted that this model should also be useful in other cases where the defects are located in different strain fields, as is the case in less perfect crystals.

For ideal point defects the capture cross section is deduced from the change in the DLTS signal ΔC as a function of filling times t_p according to[22]

$$\Delta C(t_p) = [C_0 n_T(t_p)/2N_D][\exp(-t_2 e_n) - \exp(-t_1 e_n)] = \Delta C_{max}[1 - \exp(-n\langle v_{th}\rangle \sigma_n t_p)] , \quad (9)$$

i.e., from a plot of $\log(\Delta C)$ versus t_p one can calculate σ_n if n and $\langle v_{th} \rangle$ are known. For defects in PD material experimental results show that the capture kinetics is more complicated, and as a result of experimental studies of photoconductivity in PD semiconductors, a model which discusses the capture kinetics in terms of carrier recombination to defects which are located as point defects either in the vicinity of the dislocations or, alternatively, in the dislocation core, has been proposed[26] (see Fig. 2). In this model, which has been applied to DLTS results in Ref. 5, the capture kinetics is described by a time-dependent Coulomb potential $\phi(t)$, which reflects the number of charges captured at the dislocations. The rate equation for the capture of electrons can in this case be described by[5]

$$\frac{dn_T}{dt} = (N_T - n_T) n \langle v_{th} \rangle \sigma_n \exp[-q\phi(t_p)/kT] , \quad (10)$$

an expression which is valid for all filling pulses.

B. Experimental results

Silicon samples plastically deformed at 650 °C showed a dislocation density increasing with deformation, with values ranging from 10^7–10^9 cm^{-2}, as shown in Fig. 3. For small dislocation densities, the values in Fig. 3 can be well described by the microdynamic description of creep,[27]

$$a = \frac{2b\tau_s[-A_i\sqrt{N_{dis}}/\tau_s - \ln(1 - A_i\sqrt{N_{dis}}/\tau_s)]}{KA_i^2} , \quad (11)$$

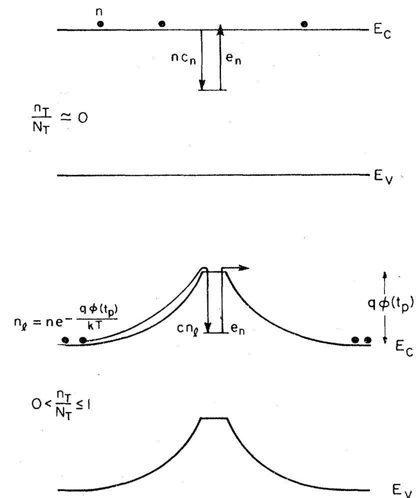

FIG. 2. An illustration of the model with point defects located inside, or around, dislocations. The situation for small occupation numbers ($n_T/N_T = 0$) resembles that for isolated point defects, while the higher occupation numbers give rise to a repulsive potential $\phi(t_p)$, which is a function of occupation of the deep levels, i.e., a function of filling time t_p during capture measurements.

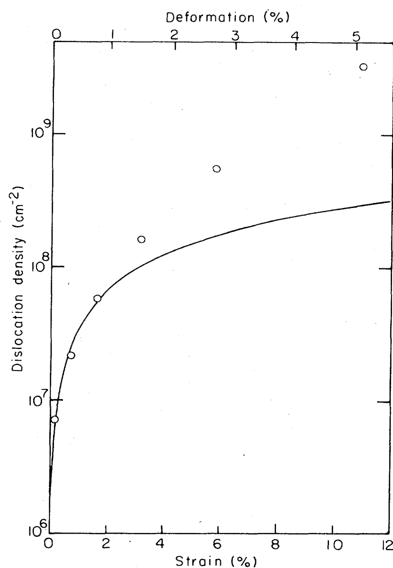

FIG. 3. The measured dislocation density as a function of deformation at 650 °C with a resolved shear stress of 30 MPa. The solid line is a theoretical fit using the microdynamic description of creep [Eq. (11)], which is valid only in the first part of the creep curve.

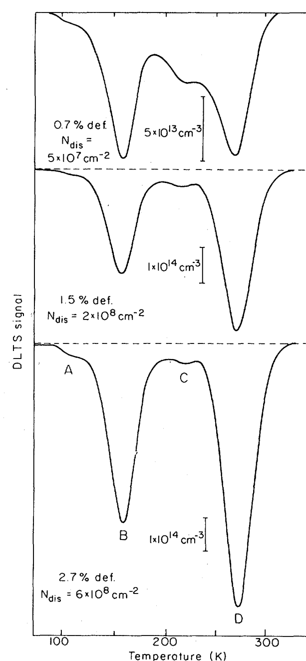

FIG. 4. DLTS spectra for differently plastically deformed n-type silicon using "standard" deformation (see Sec. II). The indicated concentrations are only approximate values since none of the correction methods mentioned in Sec. III A have been used in this figure. The gate times are $t_1=3.6$ ms and $t_2=15.6$ ms, which gives a rate window of 122 s^{-1}.

with a being the resolved shear strain, τ_s the resolved shear stress, N_{dis} the dislocation density, A_i the interaction parameter determining the maximal dislocation density ($N_{\text{dis,max}}=\tau_s^2/A_i^2$), and K a parameter which describes dislocation multiplication. The dislocation density is doubled if each dislocation moves by $\ln 2/[K(\tau_s-A_i\sqrt{N_{\text{dis}}})]$. The reduced shear stress, $\tau_s-A_i\sqrt{N_{\text{dis}}}$, is the effective shear stress acting on the moving dislocation. A good fit to the data for low dislocation densities can be obtained with

$$A_i=6.5\times10^{-4}\ \text{kg/mm},\quad K=4.8\ \text{mm/kg}\ .$$

The ansatz [Eq. (11)] describes plastic deformation in the first part of the creep curve with most dislocations being mobile. Therefore, it is not surprising that strongly deformed crystals show clear deviations which cannot be fitted satisfactorily by another choice of parameters.

For the weakly deformed material the electrical properties remained essentially the same as for the undeformed material, i.e., with a homogeneous carrier concentration corresponding to the doping level, low leakage currents, and low series resistances in the Schottky diodes. However, the deep-level concentration changed with deformation, and typical DLTS spectra from three different deformations are shown in Fig. 4. The different deformations introduced similar defect-state spectra, with apparently four traps, labeled A, B, C, and D in Fig. 4. With this type of deformation, the lines of traps B and D are always clearly resolved, while the lines of traps A and C are more complicated to analyze because of the relatively low concentrations. Traps similar to C have been previously found to dominate DLTS spectra of samples deformed at higher temperatures. Therefore, several attempts have been made to produce samples containing isolated C peaks. The DLTS spectra from samples that have been subjected to high-temperature deformation, low-temperature deformation, and annealing procedures, respectively, are shown in Fig. 5. It is obvious that the A, B, and D peaks are reduced or completely annealed, which results in a more pronounced C peak. The shape of the unusually broad C peak was found to be strongly dependent on the deformation and/or annealing treatment of the crystal and, in fact, seems to consist of at least two lines, labeled C_1 and C_2 in Fig. 5. The thermal emission rates (T^2-corrected) are—in Fig. 6—plotted versus the inverse temperature for the different peaks shown in Figs. 4 and 5, and the calculated apparent activation energies and preexponential factors can be found in Table I.

It has often been observed that the defects in PD silicon show a characteristic, nonexponential electron capture.[5] This effect is sometimes referred to as logarithmic filling since the number of filled deep levels is proportional to the logarithm of the filling time. In Fig. 7 we show how the corrected (λ-volume and strain-field broadening, see Sec. IV A) concentration of the deep levels in the space-charge region depends on the filling time t_p for the B level. For this level the logarithmic part extends over 4 orders of magnitude, and determines more than 60% of the capture to the defect. A similar result is found for the D level. For shorter filling times t_p, the capture kinetics changed for both levels and is best described in a $\log(N_T)$-versus-t_p plot. This is illustrated in Fig. 8 for the B level and in Fig. 9 for the D level.

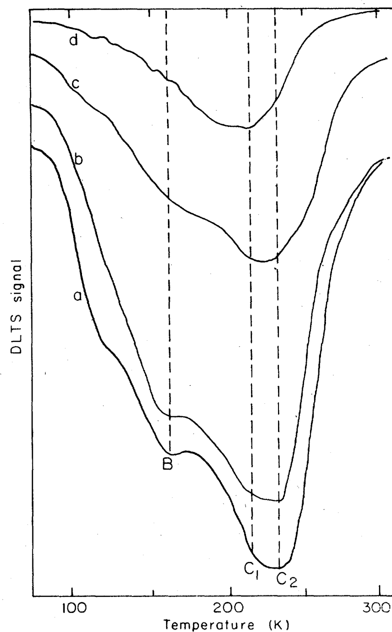

FIG. 5. DLTS spectra from samples which have been subject to different forms of treatments in order to produce isolated C lines. a, "standard" deformation (2.7%) followed by a 30-min anneal at 850 °C ($n = 4\times10^{15}$ cm^{-3}); b, deformation (2%) at 850 °C ($n = 9\times10^{15}$ cm^{-3}); c, high-stress deformation (0.2%) at 420 °C after a predeformation at 850 °C ($n = 1\times10^{15}$ cm^{-3}); d, high-stress deformation (0.2%) at 420 °C after a predeformation at 850 °C and followed by a 30-min anneal at 850 °C ($n = 1\times10^{15}$ cm^{-3}).

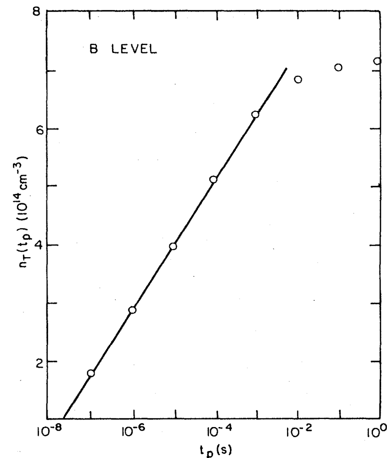

FIG. 7. The corrected concentration of filled deep levels, n_T, as a function of filling time t_p for the B level ($T = 144$ K, 1.5% deformation). The straight line indicates the region where n_T is proportional to $\ln(t_p)$, which is used for the calculations in Sec. IV A.

IV. DISCUSSION

A. DLTS results

The DLTS spectra in Figs. 4 and 5 show similar complex defect spectra as in earlier investigations of PD n-type silicon.[2–5] It should, however, be noted that the B and D levels are in our material more clearly resolved than in previous investigations, which made it possible to perform a detailed investigation of these lines. On the other hand, the A level both was disturbed by the B line and appeared in low concentrations, and could therefore not be analyzed in detail. Only Ref. 5 presents the "fingerprints," i.e., the thermal emission rates versus inverse temperature, for the different levels, making a direct comparison possible. Their data are plotted in Fig. 6, and even though their original DLTS peaks are broad and overlapping, it is clear from Fig. 6 that their plastic deformation gives rise to the same defect levels as does our material. The thermal emission rates have also been calculated directly from the DLTS spectra shown in Refs. 2 and 4, and the results are plotted in Fig. 6. Even though the activation energies given by different groups differ, it is

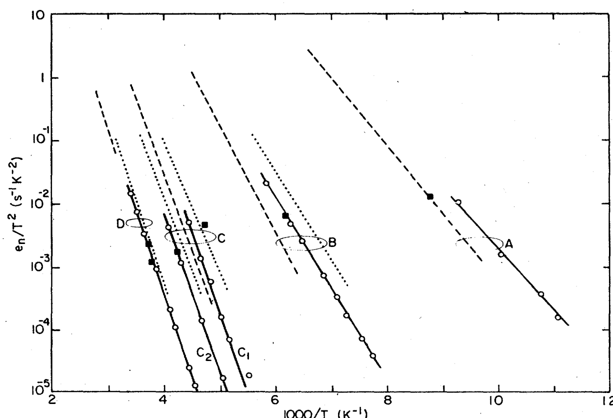

FIG. 6. Thermal emission rates (T^2-corrected) versus inverse temperature for the different DLTS peaks observed in Figs. 4 and 5 (solid lines). Also included are the data from Refs. 3 (■), 4 (dashed lines), and 5 (dotted lines).

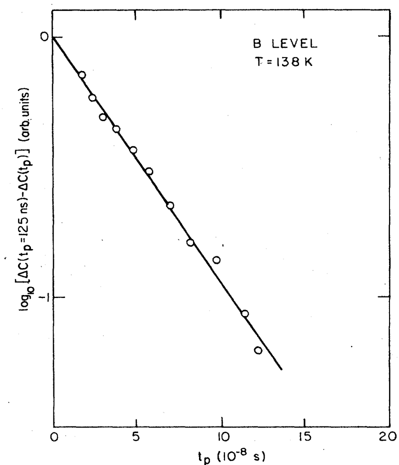

FIG. 8. The capture behavior for short filling pulses for the B level (1.5% deformation). The straight line indicates the exponential filling, according to Eq. (9).

TABLE I. Parameters of electron traps in plastically deformed silicon.

Trap	E_{a0}[a] (eV)	κ[b]	FPHW[c] (meV)	σ_n[d] (cm^2)	A_{pf}[e] (s^{-1})	σ_n[f] (cm^2)	$q\phi(t_p=100\ \mu s)$ (meV) This work	Ref. 5[g]	ΔH (eV)	$\Delta S/k$	ΔG (eV)
A	0.19				4.2×10^{6}						
B	0.29	1.78	52	1.5×10^{-16}	8.0×10^{6}	7×10^{-16}	120	180	0.29	1.3	0.31
C_1	0.52				2.9×10^{9}						
C_2	0.51				1.5×10^{8}						
D	0.54	1.18	38	2.0×10^{-16}	5.6×10^{7}	6×10^{-16}	220	360	0.54	3.2	0.61

[a]Activation energy, T^2-corrected.
[b]Correction factor of trap concentration: $N_T=\kappa N_{\text{measured}}$.
[c]Full-peak half-width, see Eqs. (8) and (9).
[d]Obtained from DLTS fitting.
[e]Prefactor: $A_{pf}=\sigma_n\langle v_{th}\rangle N_c\exp(\Delta S/k)$.
[f]Obtained from direct filling measurement.
[g]Reference 5 gives $q\phi(t_p=100\ \mu s)+\ln(n_T/N_T)$.

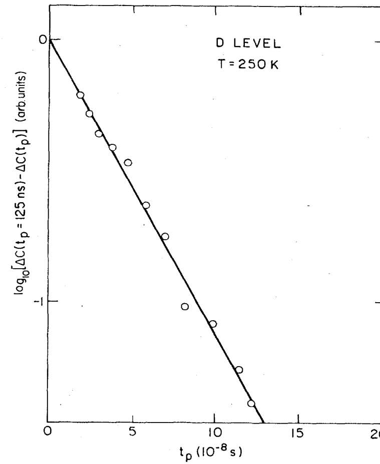

FIG. 9. The capture behavior for short filling pulses for the D level (1.5% deformation). The straight line indicates the exponential filling, according to Eq. (9).

clear from such a comparison (Fig. 6) that plastic deformation gives rise to the same group of deep energy levels in different materials. We believe this is a better way of comparing different defect-state spectra from different groups than by using only the activation energy and prefactor. For instance, the activation energy from Ref. 4 differs substantially from the values found in this paper and in Refs. 2 and 5. Their 0.18-eV line is very different in thermal emission rates (5 orders of magnitude) from our A line (0.19 eV), while their 0.28-eV line is almost identical to our A line, but very different from our 0.29-eV level (B line). This is obviously a source of great confusion when discussing these spectra, and we therefore suggest that the Arrhenius plot should be used, together with the activation energy and prefactor, as an identification mark for defects in silicon. This "standard" of comparing deep energy levels has been used for a long time in GaAs.[28]

A careful analysis of the thermally stimulated capacitance transients, and of the linewidth of the observed DLTS peaks, shows that all peaks are built up from nonexponential transients which, as already discussed in Sec. III A, make the deduced thermal emission rates, activation energies, and concentration measurements unreliable. Based on earlier suggestions on the origin of the deep levels in PD material,[29] it is now assumed that some of the deep levels are point defects located in the vicinity of, or inside, dislocations. Such deep levels would experience different strain fields, and therefore the model for broadened, deep energy levels [Eqs. (7) and (8)] would be applicable. Using as input parameters the actual DLTS setting (t_1 and t_2) and the apparent activation energy (E_{a0}) deduced from Fig. 4 (see Table I), and as fitting parameters the capture cross section (which adjusts $T_{\max}$) and broadening of the energy level (S), it is possible to fit the experimental results for the B and D levels, as shown in Figs. 10 and 11. These results suggest that the measured e_n and E_a for the B and D centers are actually the true values (within the model), and also that the concen-

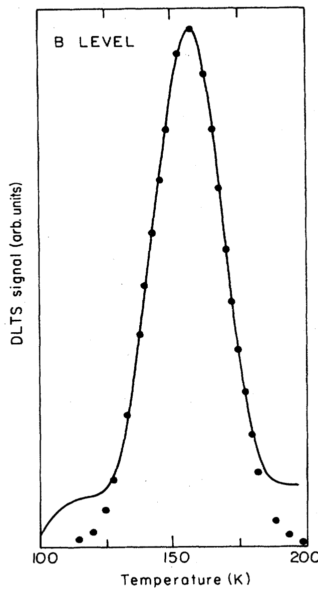

FIG. 10. Theoretical fits (●) to the experimental spectra (solid line) of the B level. The thermal activation energy $E_{a0}=0.29$ eV (from Table I), the broadening parameter $S=22$ meV, and a capture cross section of 1.5×10^{-16} cm^2 were used to adjust the peak position.

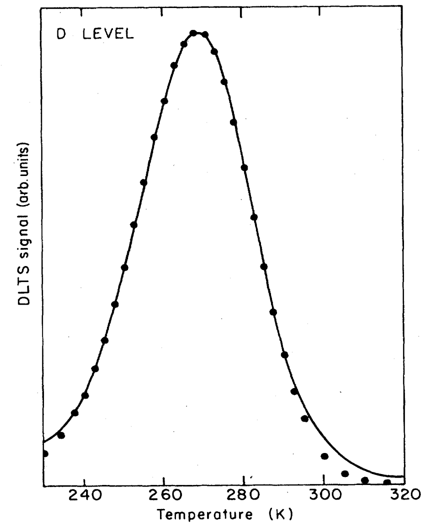

FIG. 11. Theoretical fits (●) to the experimental spectrum of the D level. The thermal activation energy $E_{a0}=0.54$ eV (from Table I), the broadening parameter $S=16$ meV, and a capture cross section of 2×10^{-16} cm^2 were used to adjust the peak position.

trations N_T, as well as the deep-level broadenings (S), can be calculated. Actually, by taking into account both this broadening effect and the λ volume [Eq. (6)], one obtains very accurate concentration determinations for these centers. All data from this fitting are presented in Table I and typical concentration values are also included in Table II.

The basic argument for assuming that the defects are located close to dislocations is the experimentally observed logarithmic capture mechanism [see Fig. 7 and Eq. (10)], which reflects the presence of a repulsive potential $\phi(t)$. Keeping in mind that our majority carriers are electrons, it is concluded that both the B and the D levels are neutral centers when empty and negatively charged when filled, i.e., acceptor levels. For small occupation numbers the potential $\phi(t)$ is expected to be small, and the capture kinetics would therefore be the same as for an ideal point defect [see Eq. (9)]. Measurements, using very short filling pulses, showed that this is in agreement with the observed data for both the B level (Fig. 8) and the D level (Fig. 9). Using Eq. (9) it is possible from these data to calculate the point-defect capture cross section for the B and D levels. The results are presented in Fig. 12, where it is shown that the capture cross section is temperature independent for both levels in the investigation temperature range. The deduced values are given in Table I.

Since we have used a $\Delta C_{\max}$ value [see Eq. (9)] which is $\Delta C_{\max}(t_p=125$ ns) when plotting the data in Figs. 8 and 9, and the filling curves nevertheless are exponential over 1 order of magnitude, we conclude that the filling of the defects is preferential, i.e., only certain defects are filled with electrons during the initial period when the filling process is point-defect-like. This might be due to the fact that some defects are located in regions where the conduction band is lower, e.g., due to strain fields (this is one way to visualize the alloy-broadening model described in Sec. III A), thus giving rise to fast capture from the percolating electrons. Another possible explanation is that once a defect has captured an electron, it prohibits further capture to near-lying defects through electrostatic repulsion. This might be possible since the defects are located

TABLE II. Defect concentrations in plastically deformed n-type Si, measured by DLTS and EPR. [4×10^{15} (P atoms)/cm^3 material, deformed at 650 °C in static compression with a resolved shear stress of 30 MPa.]

Dislocation density (cm^{-2})	Sites in the dislocation core[a] (cm^{-3})	DLTS Trap B (cm^{-3})	DLTS Trap C[b] (cm^{-3})	DLTS Trap D (cm^{-3})	EPR Si-$K1/K2$ (cm^{-3})	EPR Si-$K7$ (cm^{-3})
5×10^7	3×10^{15}	1.2×10^{14}	2.3×10^{13}	5.0×10^{13}	4.3×10^{13}	1.0×10^{13}
2×10^8	1×10^{16}	2.3×10^{14}	5.0×10^{13}	1.0×10^{14}	1.2×10^{14}	1.7×10^{13}
6×10^8	4×10^{16}	3.7×10^{14}	6.2×10^{13}	1.9×10^{14}	2.0×10^{14}	2.0×10^{13}

[a]Taking into account dissociation into two partial dislocations.

[b]The complex nature of this trap allows us only to give uncorrected, apparent concentration values.

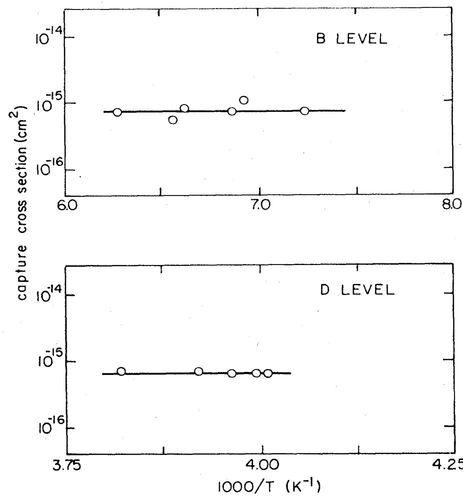

FIG. 12. Capture cross sections for electrons versus inverse temperature for the B and D levels. The straight lines indicate the temperature independence.

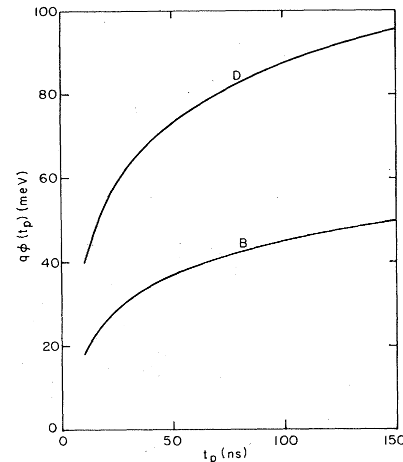

FIG. 13. The repulsive potential $q\phi(t_p)$ plotted versus filling time t_p for the B and D levels. This figure shows the behavior for short filling times.

very close to each other around (or inside) the dislocations.

The directly measured values of capture cross sections agree reasonably well with those values obtained from the fitting procedure of the broadened DLTS peaks. As shown in Table I, the values from the fitting are only 3 times lower than those measured directly. From this it is concluded that the point-defect capture cross sections are, for both levels, in a range typical for capture to neutral point defects.[30] This is in agreement with the acceptor picture as discussed above.

For long filling times t_p the electrons that are going to be captured "feel" the repulsive charges from the already captured electrons. A total negative charge is built up, and $\phi(t)$ increases to a saturation value, when all centers are filled. From Fig. 7 it is clear that $n_T = k\ln(t_p)$. This gives, together with Eq. (10),

$$q\phi(t_p) = kT[\ln(N_T - n_T)t_p n\langle v_{\text{th}}\rangle\sigma_n] - \ln(t_p\, dn_T/dt_p)\ . \tag{12}$$

Having accurate values of the concentrations and the point-defect capture cross sections σ_n, it is now possible to calculate $\phi(t)$ as a function of t_p. The results of such calculations for the B and D levels are presented in Fig. 13 for short filling times ($t_p \leq 150$ ns) and in Fig. 14 for long filling times ($t_p \leq 1$ ms). The values of $\phi(t_p = 100\ \mu\text{s})$ are compared in Table I with the value found by Kveder *et al.*,[5] who estimated the values of the potential for this filling time.

Since both the temperature dependence of the emission rates and the temperature dependence of the capture cross sections are measured, it is possible to determine the ionization enthalpies for the B and D levels. Due to the temperature independence of the capture cross sections, they are, of course, identical with the activation energies deduced from Fig. 4 and given in Table I. Using Eqs. (1) and (2), the enthalpy from Fig. 4, and the prefactor given in Table I, it is furthermore possible to estimate the entropy and calculate Gibbs's free energy. These calculated values are presented in Table I.

Despite the many similarities between the B and D levels, they must, however, be due to distinctly different defects, as their relative concentration is strongly dependent on the dislocation density. Samples with small dislocation densities, and especially with dominantly straight dislocations, contain only small or even undetectable concentrations of the D trap, whereas the concentration of the B trap scales quite well with the dislocation density.

An interesting question is whether the dislocation properties influence the basic physical properties of the isolated point defects. If so, the expression for detailed balance, Eq. (1), should be modified to [see Eq. (10)]

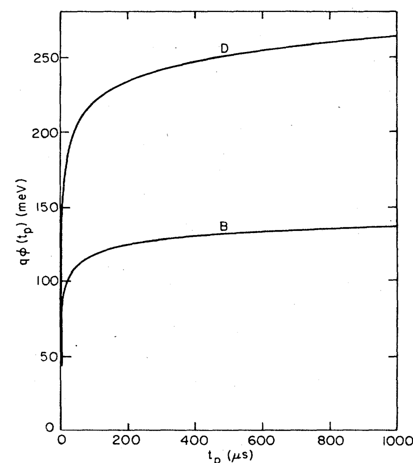

FIG. 14. The repulsive potential $q\phi(t_p)$ plotted versus filling time t_p for the B and D levels. This figure shows the behavior for long filling times.

$$e_n = \sigma_n \langle v_{\text{th}} \rangle N_c \exp(-\Delta G/kT) \exp[-\phi(t)q/kT] \; . \tag{13}$$

Since the capture is strongly dependent on the filling time t_p, the emission would be as sensitivie to the filling time used during the measurements. The difference in activation energies measured with long and short filling times would therefore be about $q\phi(t)$, i.e., 140 meV for the B level and 260 meV for the D level (see Fig. 14). Measurements, using 0.1-s and 100-ns filling pulses, showed, however, no difference in the emission rates or in the activation energies for the two defects. This indicates that Eq. (1) is the valid expression for the point defects investigated, and that the dislocations influence the measurements of the point-defect properties rather than the properties themselves (compare Fig. 2).

The broad C line appears in all samples containing dislocations, and is thermally stable even up to 900 °C. As is shown in Fig. 5, the C line consists of at least two different lines, C_1 and C_2, which can be separated by using different filling times during the measurement. These lines show properties which are clearly different from the B and D lines. It was, for instance, not possible to fit the experimental data on the C lines with the deep-level broadening model [Eq. (7)], and the time dependence of the capture process cannot be perfectly described with the models described in Sec. III A. It is, however, interesting to note that the activation energies for C_1 and C_2 are very similar, while the prefactors are very different. One possible interpretation is that the two lines originate from identical defects located in different surroundings in the crystal, which could give rise to different capture cross sections (i.e., different prefactors). This is in agreement with the observations (Fig. 5) that different treatments of the crystal produce different concentrations of the two lines. The C line has been shown to be produced in direct proportion to the dislocation density,[3] and the corresponding defect has therefore been suggested to be located in the dislocation. It should also be noted that the values (e_n, E_a, and N_T) determined for the C_1 and C_2 lines (and the A line) are apparent values, since the origin for the nonexponentiality of the measured capacitance signal is unknown in these cases.

B. Comparison with EPR

The EPR spectra of plastically deformed silicon have been described in detail recently.[6,14] In summary, "standard" plastic deformation of undoped silicon results in the formation of at least seven distinguishable EPR centers, of which only four have been investigated in detail, namely Si-$K1/K2$ and Si-$K3$,-$K4$,-$K5$. The spectra Si-Y (Ref. 13) and Si-rt (Ref. 14) contain the largest numbers of unpaired spins. The Si-$K1/K2$ spectrum can be ascribed to a well-defined dangling-bond center in the core of the dislocations. This defect occurs in three charge states, with zero (diamagnetic, no EPR signal), one ($S=\frac{1}{2}$, Si-$K1$), or two ($S=1$, Si-$K2$) electrons. Photo-EPR studies[31] allowed its energy levels to be located near the middle of the band gap. Both the Si-Y spectrum as well as the Si-$K1$ spectrum are shown in Fig. 15. The Si-$K3$, Si-$K4$, and Si-$K5$ spectra show no relation to the dislocations. They have therefore been identified with point-defect clusters produced during the deformation. The Si-$K6$ and Si-K7 EPR spectra occur only in p- or n-type silicon, respectively. They can be ascribed to impurity atoms in the dislocation core.[6]

Samples deformed at high temperatures ($T > 0.6T_m$) and samples annealed at high temperature after "standard" deformation exhibit only a small fraction of the Si-Y broad line. This remaining, thermally stable part has been labeled Si-R in Ref. 14. Deformation at low temperatures but under high stress (e.g., 420 °C, 300 MPa) results predominantly in straight dislocations. These samples with small total dislocation density ($\sim 10^7$ cm^{-2}) do not show any of the dangling-bond-type EPR centers (i.e., Si-$K1$ to Si-$K5$ and Si-Y). In doped material, however, this kind of deformation produces Si-$K6$ or Si-$K7$ centers. Very recent investigations of crystals deformed in this way, but up to high dislocation densities, showed the appearance of the Si-$K1/K2$ centers with concentration proportional to the shear strain.[14]

Comparing the DLTS spectra with the EPR spectra, only the DLTS line D, which is dominant in strongly deformed silicon ("standard" deformation, high dislocation density), shows characteristics wich are comparable to Si-$K1/K2$. Both are produced during deformation at intermediate temperatures and anneal at 800 °C. Photo-EPR of Si-$K1/K2$ directly showed the existence of a midgap level of this center.[31] In addition, the concentrations of the EPR center Si-$K1/K2$ compare well to the DLTS line D, see Table II. A correlation of the DLTS D line with the point-defect spectra Si-$K3$,-$K4$,-$K5$, which appear in concentrations similar to Si-$K1/K2$, cannot be definitely ruled out at present. However, Si-$K3$,-$K4$,-$K5$ have all

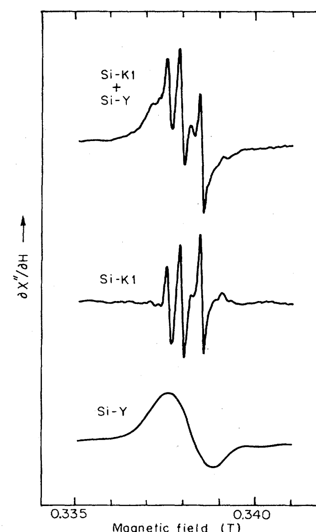

FIG. 15. The EPR signals from "standard" deformation show a mixed signal from the Si-Y and Si-$K1$ spectra. These signals have been separated by omitting certain parts of the spectrum obtained by Fourier transformation, and subsequent inverse Fourier transformation of the separated parts (Ref. 32).

been identified as point-defect clusters not influenced by dislocations.[11] On the other hand, the DLTS *D* line clearly shows logarithmic filling behavior characteristic of a defect inside or close to dislocations, so that the correlation of the *D* line with Si-*K*1/*K*2 appears to be more likely.

The DLTS *C* lines appear even in silicon crystals deformed or annealed at high temperatures. Thus the only corresponding EPR spectrum is the thermally stable part of the broad background, i.e., the Si-*R* line. This Si-*R* defect seems to be directly related to dislocations, as it is detectable in all samples containing dislocations. Its concentration could not yet be precisely determined because of the complex relaxation behavior of this spectrum.[14] Since the *C* line (DLTS) also is directly proportional to the dislocation density,[3] it appears likely that the *C* line and the Si-*R* spectrum originate from the same defect at dislocations. Its microscopic nature, however, is not yet clear.

The *B* line in the DLTS spectrum appears in the same samples, in which the Si-*K*7 spectrum can be detected. Photo-EPR of Si-*K*7 indicated the energy level of this defect to be less than 0.4 eV from the conduction band. However, the concentration of Si-*K*7 is about an order of magnitude smaller than the concentration of the *B* trap. This casts some doubt on the identification of Si-*K*7 with the *B* line suggested previously.[6] The concentration difference might, however, be explained by the sensitivity of the EPR signal to small distortions in the surroundings of a dangling-bond electron. A large fraction of the defect might be slightly distorted because part of the defects are located at places of different strain fields or nearby defects like other dislocations, which distort the DLTS lines only slightly but broaden the EPR signal very much. If this is the case only a fraction of the DLTS centers would give rise to well-defined EPR signals. This model is supported by the considerable line broadening observed for the DLTS *B* line. Further experimental data are needed for a final decision on this question.

V. CONCLUSIONS

DLTS measurements of deep energy levels in PD *n*-type silicon show that different types of defects are created. First, there are point defects located in the vicinity of, or inside, the dislocations, which therefore show broad peaks and unusual filling behavior. Strong evidence has been given that the *B* and *D* levels are of this type. Analysis of these levels in a point-defect model has revealed that these acceptor levels are broadened in a strain field of the dislocations, that the levels have well-defined emission rates, and that the levels have temperature-independent capture cross sections with magnitudes typical for neutral defects. Furthermore, the enthalpy, entropy, and Gibbs free energy for the point defects have been determined, and improved concentration determinations have been used to investigate how the dislocation properties influence the capture kinetics of the point defects. The observed logarithmic capture process has been described in a model, characterized by a Coulombic potential $\phi(t)$, which has been determined as a function of the filling time of the defects.

Second, there are another type of defect (the *C* lines) which shows, in many respectve, different properties compared to those discussed above. Its filling behavior is very complex and cannot be determined unambiguously. It occurs in all samples containing dislocations and its concentration is roughly proportional to the dislocation density, as already observed previously in Ref. 3. It is therefore believed to be directly related to the dislocations.

From a comparison of the DLTS lines with the EPR centers, it is argued that the *D* line (DLTS) can be correlated with the Si-*K*1/*K*2 "dangling-bond" center. This is supported by formation and annealing behavior, the energy level determined by photo-EPR, and from the measured concentrations.

It is also suggested that the *C* line might be related to the Si-*R* center.[14] This is based on the observed stability upon annealing, and the direct correlation with dislocations, which has been established for both defects.

The suggested correlation of the *B* line (DLTS) with the Si-*K*7 center does not appear to be supported by the measured defect concentrations. EPR spin densities are about an order of magnitude lower than the concentrations established for the *B* line. An explanation which can solve this discrepancy has been suggested, involving lack of EPR detection of part of the defects due to strain broadening.

This paper might establish a basis for further qualitative and quantitative work in this field toward a microscopic understanding of the electrically active defects at dislocations in silicon.

ACKNOWLEDGMENTS

The authors want to thank C. Kisielowski-Kemmerich for stimulating discussions and a critical reading of the manuscript. This work was supported in part by the Director, Office of Basic Energy Research, Office of Basic Energy Sciences, Materials Sciences Division of the U.S. Department of Energy, under Contract No. DE-AC03-76SF00098. It was also supported in part by the Deutsche Forschungsgemeinschaft.

*Also at Department of Materials Science, University of California, Berkeley, CA 94720.

[1]R. H. Glaenzer and A. G. Jordan, Solid-State Electron. **12**, 247 (1969).

[2]L. C. Kimerling and J. R. Patel, Appl. Phys. Lett. **34**, 73 (1979).

[3]J. R. Patel and L. C. Kimerling, Cryst. Res. Technol. **16**, 187 (1981).

[4]W. Szkielko, O. Breitenstein, and R. Pickenhein, Cryst. Res. Technol. **16**, 197 (1981).

[5]V. V. Kveder, Y. A. Ossipyan, W. Schroter, and G. Zoth, Phys. Status Solidi A **72**, 701 (1982).

[6]E. R. Weber and H. Alexander, J. Phys. (Paris) Colloq. **44**, C4-319 (1983).

[7]W. Schroter and M. Seibt, J. Phys. (Paris) Colloq. **44**, C4-329 (1983).

[8]A. Ourmazd, Contemp. Phys. **25**, 251 (1984).
[9]H. Ono and K. Sumino, J. Appl. Phys. **57**, 287 (1985).
[10]W. Schröter, in *Defects and Radiation Effects in Semiconductors, 1978,* edited by J. H. Albany (Institute of Physics, Bristol, 1979), p. 114.
[11]E. R. Weber and H. Alexander, J. Phys. (Paris) Colloq. **40**, C6-101 (1979).
[12]V. V. Kveder and Yu. A. Osip'yan, Zh. Eksp. Teor. Fiz. **80**, 1206 (1981) [Sov. Phys.—JETP **53**, 618 (1981)].
[13]M. Suezawa, K. Sumino, and M. Iwaizumi, in *Defects and Radiation Effects in Semiconductors, 1980,* edited by R. R. Hasiguti (Institute of Physics, Bristol, 1981), p. 407.
[15]N. A. Drozdov, A. A. Patrin, and V. D. Tkachev, Pis'ma Zh. Teor. Fiz. **23**, 651 (1976) [JETP Lett. **23**, 597 (1976)].
[16]M. Suezawa and K. Sumino, J. Phys. (Paris) Colloq. **44**, C4-133 (1983).
[17]R. Sauer, J. Weber, J. Stoltz, E. R. Weber, K. H. Kusters, and H. Alexander, Appl. Phys. A **36**, 1 (1984).
[18]K. Wessel and H. Alexander, Philos. Mag. **35**, 1523 (1977).
[19]U. Schmidt, E. Weber, H. Alexander, and W. Sander, Solid State Commun. **14**, 735 (1974).
[20]L. Jansson, V. Kumar, L. A. Ledebo, and K. Nideborn, J. Phys. E **14**, 464 (1981).
[21]O. Engstrom and A. Alm, Solid-State Electron. **21**, 1571 (1978).
[22]H. G. Grimmeiss and C. Ovren, J. Phys. E **14**, 1032 (1982).
[23]D. V. Lang, J. Appl. Phys. **45**, 3014 (1974); **45**, 3023 (1974).
[24]D. V. Lang, in *Thermally Stimulated Relaxation in Solids,* Vol. 37 of *Topics in Applied Physics,* edited by P. Braunlich (Springer, Berlin, 1979).
[25]P. Omling, L. Samuelson, and H. G. Grimmeiss, J. Appl. Phys. **54**, 5117 (1983).
[26]T. Figielski, Phys. Status Solidi **6**, 529 (1964).
[27]H. Alexander and P. Haasen, in *Solid State Physics,* edited by F. Seitz, D. Turnbull, and H. Ehrenreich (Academic, New York, 1968), Vol. 22, p. 28.
[28]G. M. Martin, A. Mitonneau, and A. Mircea, Electron Lett. **13**, 191 (1977).
[29]E. Weber and H. Alexander, in *Radiation Effects in Semiconductors, 1976,* edited by N. B. Urli and J. W. Corbett (Institute of Physics, Bristol, 1977), p. 266.
[30]J. Bourgoin and M. Lannoo, in *Point Defects in Semiconductors II* (Springer, Berlin, 1983), p. 196.
[31]R. Erdmann and H. Alexander, Phys. Status Solidi A **55**, 251 (1979).
[32]C. Kisielowski-Kemmerich and J. Michel (unpublished).